CHEMISTRY OF MATERIALS

Article

pubs.acs.org/cm

Enhancing the Hardness of Superhard Transition-Metal Borides: Molybdenum-Doped Tungsten Tetraboride

Reza Mohammadi,[*,†] Christopher L. Turner,[‡] Miao Xie,[‡] Michael T. Yeung,[‡] Andrew T. Lech,[‡] Sarah H. Tolbert,[‡,§,∥] and Richard B. Kaner[*,‡,§,∥]

[†]Department of Mechanical and Nuclear Engineering, Virginia Commonwealth University, Richmond, Virginia 23284, United States
[‡]Department of Chemistry and Biochemistry, [§]Department of Materials Science and Engineering, and [∥]California NanoSystems Institute (CNSI), University of California, Los Angeles (UCLA), Los Angeles, California 90095, United States

ABSTRACT: By creation of solid solutions of the recently explored low-cost superhard boride, tungsten tetraboride (WB_4), the hardness can be increased. To illustrate this concept, various concentrations of molybdenum (Mo) in WB_4, that is, $W_{1-x}Mo_xB_4$ (x = 0.00−0.50), were systematically synthesized by arc melting from the pure elements. The as-synthesized samples were characterized using energy-dispersive X-ray spectroscopy (EDS) for elemental analysis, powder X-ray diffraction (XRD) for phase identification, Vickers microindentation for hardness testing, and thermal gravimetric analysis for determining the thermal stability limit. While the EDS analysis confirmed the elemental purity of the samples, the XRD results indicated that Mo is completely soluble in WB_4 over the entire concentration range studied (0−50 at. %) without forming a second phase. When 3 at. % Mo is added to WB_4, Vickers hardness values increased by about 15% from 28.1 ± 1.4 to 33.4 ± 0.9 GPa under an applied load of 4.90 N and from 43.3 ± 2.9 to 50.3 ± 3.2 GPa under an applied load of 0.49 N. Thermal gravimetric analysis revealed that the powders of this superhard solid solution, $W_{0.97}Mo_{0.03}B_4$, are thermally stable in air up to ∼400 °C. These results indicate that the hardness of superhard transition-metal borides may be enhanced by making solid solutions with small amounts of other transition metals, without introducing a second phase to their structures.

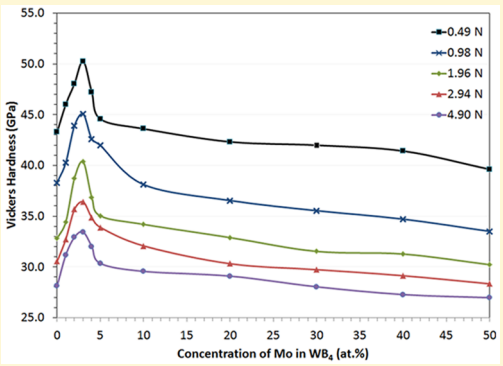

1. INTRODUCTION

The concept of creating superhard borides by incorporating boron into the dense structure of transition metals such as ruthenium (Ru), osmium (Os), and rhenium (Re) has become well-established over the past few years.[1,2] With increasing demand for high-performance and long-lasting cutting and forming tools, the members of this expanding class of superhard metals hold promise to address the shortcomings of traditional tool materials. Those shortcomings include their high cost (silicon nitride, cubic boron nitride, and diamond), their inability to cut ferrous metals due to chemical reactions (diamond), instability in the presence of humidity (cubic boron nitride), and relatively low hardness (tungsten carbide).[3] In contrast, rhenium diboride (ReB_2) has demonstrated exciting properties including high hardness (>40 GPa),[4] the ability to scratch diamond,[5] excellent electrical conductivity,[6] a high shear modulus (267−273 GPa),[7−9] and straightforward synthesis under ambient pressure.[5] Unfortunately, however, rhenium is a member of the platinum group metals and, therefore, is prohibitively expensive. The ongoing search for new superhard borides with increased hardness and reduced cost of production has recently led to tungsten tetraboride (WB_4), an inexpensive member of this growing family of superhard materials.

Although some early studies looked at the synthesis and crystallography of WB_4,[10,11] its superhard nature was not explored until 2002 by Brazhkin et al.[12] After we discussed the potential applications of this superhard boride in a *Science* perspective in 2005,[1] a few studies examined its mechanical properties both in bulk and thin film form.[13−15] Recently, we examined the hardness and high-pressure behavior of WB_4 in some detail.[16,17] Using microindentation, nanoindentation, and in situ high-pressure X-ray diffraction, we measured a Vickers hardness of 43.3 GPa (under an applied load of 0.49 N), a nanoindentation hardness of 40.4 GPa (at a penetration depth of 250 nm), and a bulk modulus of 326−339 GPa for WB_4 samples synthesized by arc melting at ambient pressure.[16] Under an extremely high pressure of ∼42 GPa (∼415000 atm), WB_4 exhibits a unique second-order phase transition that can be attributed to its very strong but nonflexible cagelike crystal structure.[17,18] Additionally, we showed that by adding ∼1 at. % rhenium (Re) to WB_4, the Vickers hardness (under a 0.49 N applied load) increases from 43.3 to 49.8 GPa due to a dispersion hardening mechanism obtained from the formation of an ReB_2-type second phase. This work thus showed that an extrinsic component could modify the hardness in this system.[16]

Although the formation of a second phase is one way to enhance the mechanical properties, single-phase materials are

Received: November 11, 2015
Revised: December 15, 2015
Published: December 21, 2015

DOI: 10.1021/acs.chemmater.5b04410
Chem. Mater. 2016, 28, 632−637

usually preferred because of the nonuniformity that the second phase introduces in the structure of the matrix. Solid-solution hardening is often considered as an alternative route to improve the hardness and other mechanical properties of crystalline materials without adding an extrinsic component to the structure and properties of the host material.[19] This hardening method can arise from two entirely different mechanisms: size mismatch[20] and/or valence electron count difference[21] between the atoms of solute and solvent. Indeed, the formation of solid solutions of hard ruthenium diboride (RuB_2) with osmium (Os) previously demonstrated some promising improvements in hardness.[22] In a recent study, we used a similar approach to examine the possibility of further enhancing the hardness of WB_4 by individually doping it with 0−50 at. % tantalum (Ta), manganese (Mn), and chromium (Cr).[23] We found that when Ta and Mn are each added to WB_4, three very distinct increases were seen in its Vickers hardness curves, under all applied loads between 0.49 and 4.90 N, when plotted against composition (0−50 at. % Ta or Mn). A sharp increase in hardness at low concentrations of ∼2 at. % Ta or 4 at. % Mn was observed and attributed to the valence electron difference between W (group 6) and Ta (group 5) or Mn (group 7); the two broad peaks at maximum solubility (∼20 at. % Ta or Mn) and high concentrations (∼40 at. % Ta or Mn) were associated with atomic size mismatches between W (1.41 Å) and Ta (1.49 Å) or Mn (1.32 Å),[24] with changes in interfaces between grains, and with dispersion hardening from TaB_2 or MnB_4, respectively.

In the case of chromium (Cr) in WB_4, however, only two hardness peaks were seen at ∼10 and 40 at. % Cr. While the broad peak at ∼40 at. % Cr was clearly due to the dispersion hardening of CrB_2 and CrB_4, we could not draw certain conclusions about the origin of the relatively broad peak that was observed at ∼10 at. % Cr. The maximum solubility of Cr in WB_4 is ∼10 at. % Cr, so it is unclear if this peak is due to the atomic size mismatch between W (1.41 Å) and Cr (1.30 Å)[24] at maximum solubility, to electronic structure changes, despite the fact that W and Cr are isoelectronic (group 6), or to some interfacial/grain boundary effects. Conversely, understanding the answer to this question is a key component of our ability to create new hard solid solutions based on rational design.

To clarify this, we have embarked on the current study, where we have designed a similar, but much cleaner, system, by creating solid solutions of molybdenum (Mo) in WB_4. Lying in the same column of the Periodic Table (group 6), Mo has the same number of valence electrons as W and Cr. In addition, since Mo has a close atomic radius to W (W = 1.41 Å, Mo = 1.39 Å, note B = 0.78 Å)[24] and both WB_4 and MoB_4 are hexagonal and crystallize in the $P6_3/mmc$ space group, with almost identical lattice parameters,[10,16,23,25] one would expect to obtain an extended range where solid solutions of Mo in WB_4 can be created. These facts should lead to the absence of solid-solution hardening due to either atomic size mismatch or dispersion hardening from a second phase. In this work, we, thus, report the synthesis of molybdenum-doped tungsten tetraboride solid solutions containing a broad range of Mo concentrations varying from 0 to 50 at. % (i.e., $W_{1-x}Mo_xB_4$ with x = 0.00−0.50). An investigation of the changes in load-dependent Vickers hardness across the entire solubility range of Mo from 0 to 50 at. % indicates that the hardness of WB_4 can be significantly increased by adding Mo to WB_4, and the underlying hardening mechanism(s) can be understood.

2. EXPERIMENTAL PROCEDURE

To synthesize the samples in each concentration, powders of pure tungsten (99.95%, Strem Chemicals, Newburyport, MA, USA), molybdenum (99.9%, Strem Chemicals), and amorphous boron (99+%, Strem Chemicals) were blended thoroughly using a digital vortex mixer, followed by grinding in an agate mortar and pestle set, to achieve a uniform mixture. The ratio of boron to tungsten was kept constant at 12:1 in all samples to stabilize the structure of WB_4 and inhibit the formation of the thermodynamically favorable phase, tungsten diboride (WB_2).[10,16] The mixture was then compacted to a pellet in a steel die using a hydraulic Carver press and applying a pressure of ∼2000 lb. The pellets each weighing ∼500 mg were synthesized, under high-purity argon at ambient pressure, in a homemade arc-melting furnace using a maximum applied alternating current of ∼130 A sustained for ∼3 min. The pellets were arced until completely molten and homogenized, with temperatures reaching well above 2020 °C, which is the melting point of WB_4. The as-synthesized ingots were dissected using a sinter-bonded diamond lapidary sectioning saw (South Bay Technology Inc., San Clemente, CA, USA). Half of each ingot was crushed into a fine powder, using a hardened-steel mortar and pestle set, for powder X-ray diffraction and thermal gravimetric experiments. The other half was mounted in epoxy at room temperature using a cold-mount resin and hardener epoxy set (Allied High Tech Products Inc., Rancho Dominguez, CA, USA). The mounted sample was polished with a tripod polisher (South Bay Technology Inc.) using polishing papers of grit sizes ranging from 120 to 1200 (Allied High Tech Products Inc.), followed by abrasive films containing diamond particles ranging from 30−0.5 μm in size (South Bay Technology Inc.), to achieve an optically smooth surface for elemental analysis and hardness testing.

Energy-dispersive X-ray spectroscopy (EDS) and powder X-ray diffraction (XRD) were used to examine the elemental composition and phase purity of the samples, respectively. EDS analysis was carried out on the polished samples using an energy-dispersive X-ray analysis detector mounted on a scanning electron microscope (JEOL JSM 6700 F, Japan). For phase identification, powder XRD was performed on the crushed-to-powder samples using an X'Pert Pro powder X-ray diffraction system (PANalytical, Almelo, The Netherlands). XRD patterns were collected from the powder samples using a $Cu_{K\alpha}$ X-ray radiation (λ = 1.5418 Å) and the following scan settings: scan range 2θ = 10−140 deg, step size 0.0167°, time per step 85.1 s, and scan speed 0.025 deg/s The patterns were then compared with reference patterns available in the Joint Committee on Powder Diffraction Standards (JCPDS) database to determine the phases present in the samples.

Once the purity of the samples was confirmed, we performed hardness testing on the polished samples. Hardness measurements were carried out using a MicroMet 2103 microindentation system (Buehler Ltd., Lake Bluff, IL, USA) equipped with a pyramid diamond indenter tip with Vickers geometry. To study the load-dependent hardness of WB_4−Mo solid solutions, five different loads of 0.49 (low load), 0.98, 1.96, 2.94, and 4.90 N (high load) were applied to the surface of the samples with a dwell time of 15 s. To ensure accurate measurements, the samples were indented at least 20 times at randomly chosen spots under each load. The lengths of the diagonals of the impression marks, created by the indenter on the surface of the samples, were then measured using a high-resolution Zeiss Axiotech 100HD optical microscope (Carl Zeiss Vision GmbH, Aalen, Germany) under a total magnification of 500×. The Vickers microindentation hardness values (H_V, in GPa), under various applied loads, were calculated using the equation[16]

$$H_V = 1854.4P/d^2 \quad (1)$$

where P is the applied load in Newtons (N) and d is the arithmetic mean of the diagonals of the indent mark in micrometers.

Thermal gravimetric analysis was utilized to test the thermal stability of the hardest solid solution in the WB_4−Mo system, $W_{0.97}Mo_{0.03}B_4$. Using a Pyris Diamond thermogravimetric/differential thermal analyzer unit (TG-DTA, PerkinElmer Instruments, Waltham, MA, USA), a powder sample of this superhard solid solution was

DOI: 10.1021/acs.chemmater.5b04410
Chem. Mater. 2016, 28, 632−637

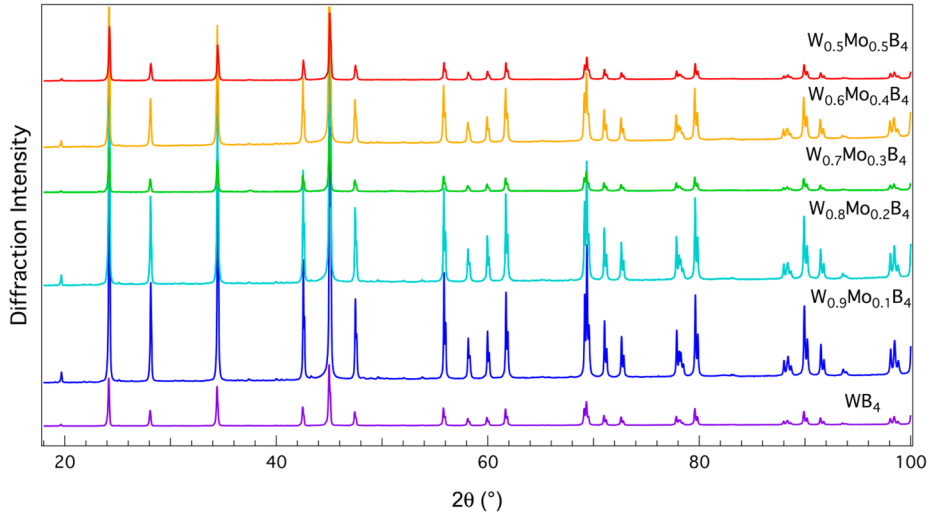

Figure 1. Selected X-ray diffraction patterns of tungsten tetraboride (WB_4) solid solutions with molybdenum (Mo). The bottom pattern corresponds to pure WB_4 (JCPDS, reference code: 00-019-1373). These patterns show that Mo is completely soluble in WB_4 over the entire composition range studied from 0 to 50 at. %.

Table 1. Lattice Parameters and Important *d*-Spacings for WB_4 and Its Selected Solid Solutions with Mo, as Measured Using Powder X-ray Diffraction[a]

compound	a (Å)	c (Å)	V (Å^3)	d_{100} (Å)	d_{101} (Å)	d_{002} (Å)	d_{110} (Å)	d_{112} (Å)
WB_4	5.1985(4)	6.3371(7)	148.32	4.5020(7)	3.6701(7)	3.1685(6)	2.5992(7)	2.0096(0)
$W_{0.97}Mo_{0.03}B_4$	5.1991(6)	6.3370(1)	148.34	4.5025(1)	3.6703(8)	3.1687(9)	2.5995(2)	2.0097(0)
$W_{0.95}Mo_{0.05}B_4$	5.1997(2)	6.3379(3)	148.40	4.5030(5)	3.6708(5)	3.1689(4)	2.5998(4)	2.0099(6)
$W_{0.90}Mo_{0.10}B_4$	5.2001(3)	6.3386(5)	148.44	4.5033(8)	3.6711(6)	3.1692(9)	2.6000(3)	2.0101(4)
$W_{0.80}Mo_{0.20}B_4$	5.2003(1)	6.3391(3)	148.46	4.5035(5)	3.6713(5)	3.1695(4)	2.6001(3)	2.0102(5)
$W_{0.70}Mo_{0.30}B_4$	5.2004(5)	6.3396(6)	148.48	4.5036(4)	3.6715(2)	3.1698(4)	2.6001(8)	2.0103(5)
$W_{0.60}Mo_{0.40}B_4$	5.2011(3)	6.3398(1)	148.52	4.5042(4)	3.6718(3)	3.1698(1)	2.6005(2)	2.0105(0)
$W_{0.50}Mo_{0.50}B_4$	5.2012(3)	6.3400(5)	148.53	4.5043(4)	3.6719(6)	3.1700(1)	2.6005(8)	2.0105(8)

[a]Error values are given in parentheses.

heated up to 200 °C in air, at a rate of 20 °C/min, and soaked at this temperature for 20 min to remove any moisture. The sample was then heated to 1000 °C at a rate of 2 °C/min and held at this temperature for 120 min. The sample was next air-cooled to room temperature at a rate of 5 °C/min. To compare the thermal stability of this solid solution with that of a conventional cutting tool material, we repeated our TGA experiment on a tungsten carbide powder sample (WC, 99.5%, Strem Chemicals) in air using the same experimental conditions. The solid products of the thermal reactions were identified using powder X-ray diffraction.

3. RESULTS AND DISCUSSION

EDS confirmed the absence of any impurity elements or secondary metal boride phases in the as-synthesized samples. Using this technique, we also verified the desired stoichiometry of the elements comprising the samples synthesized at each concentration, 0−50 at. % Mo in WB_4. A selection of the XRD patterns of the synthesized compounds in the WB_4−Mo system is shown in Figure 1.

Figure 1 shows that single-phase solid solutions of Mo in WB_4 can be formed over the entire composition range studied (0−50 at. %). The bottom pattern corresponds to WB_4 (JCPDS, reference code: 00-019-1373) and no softer impurity phases such as WB_2 (which has major peaks at 2θ = 25.683°, 34.680°, and 35.275°) are observed. All samples, however, do contain some extra crystalline boron that is not observable within the resolution of our powder X-ray diffraction instrument. Our previous work with neutron diffraction has unequivocally shown that excess boron is needed for the synthesis of phase-pure WB_4 and crystallizes from the melt as rhombohedral β-boron.[18] Table 1 reports the experimental lattice parameters and important *d*-spacings for a number of WB_4−Mo solid solutions from powder X-ray diffraction. It can be observed from the data in this table that the lattice parameters of WB_4 increase almost linearly with the addition of Mo, with R^2 values of 0.85 for a, 0.86 for c, and 0.86 for V. Similar trends are seen for the changes for each individual sample in the *d*-spacing.

The changes in Vickers hardness for solid solutions of Mo in WB_4, under loads ranging from 0.49 to 4.90 N, are shown in Figure 2. All solid solutions display a clear indentation size effect, where indent size (and thus hardness) is dependent on the applied load. This phenomenon, which has also been observed in the hardness behavior of other superhard borides,[2,5,22] is an inherent property of these compounds and likely arises from the load-dependent opening of new slip systems, from an elastic-plastic deformation transition, and/or from initiation and propagation of subsurface cracks.[2,16] It is also observed from Figure 2 that the Vickers hardness, under an applied load of 0.49 N (low load), starts at 43.3 ± 2.9 GPa for pure WB_4, and then shows a relative sharp increase in hardness that peaks at 50.3 ± 3.2 GPa with a concentration of just 3 at. % Mo. After the peak, the hardness decreases almost linearly with a very gradual slope to a value of 39.6 ± 0.94 GPa for 50 at. % Mo addition. Similar trends are seen for the other hardness

DOI: 10.1021/acs.chemmater.5b04410
Chem. Mater. 2016, 28, 632−637

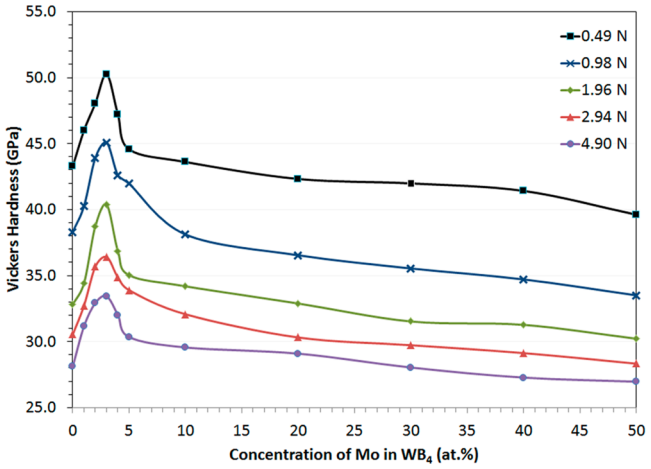

Figure 2. Vickers hardness of WB_4 solid solutions with Mo, ranging in concentration from 0 to 50 at. %, under applied loads of 0.49 (low load), 0.98, 1.96, 2.94, and 4.90 N (high load). The standard deviations of the mean hardness values under the applied loads of 0.49, 0.98, 1.96, 2.94, and 4.90 N are, respectively, within 3.51, 3.41, 2.72, 1.88, and 1.79 GPa.

loads (0.98, 1.96, 2.94, and 4.90 N). For example, Vickers hardness under high load (4.90 N) shows a 15.9% increase from 28.1 ± 1.4 GPa for pure WB_4 to 33.4 ± 0.9 GPa at $W_{0.97}Mo_{0.03}B_4$; after the peak, it again decreases linearly to 26.0 ± 0.8 GPa for the $W_{0.50}Mo_{0.50}B_4$ solid solution. The high-load hardness of the hardest solid solution in this series ($W_{0.97}Mo_{0.03}B_4$, H_V = 33.4 GPa) is at least 23% higher than that of the conventional cutting tool material, WC, with a Vickers hardness of 25.6 GPa measured under an applied load of 9.80 N.[3]

Since our EDS area mapping and XRD results (Figure 1 and Table 1) have eliminated the formation of any second phase(s) during the synthesis of the samples, the complete solubility of Mo in WB_4 argues strongly against the idea that dispersion/precipitation hardening is at the root of the sharp hardness peak present at ∼3 at. % Mo in Figure 2. Moreover, it appears unlikely that the hardening arises from size mismatch effects. This conclusion is based both on the close atomic radii of W (1.41 Å) and Mo (1.39 Å)[24] and on the fact that hardening due to atomic size mismatch generally appears as a broad deviate from Vegard's law near the end of the solubility region.[23,26] The sharp peak in hardness seen at a low concentration of 3 at. % Mo in WB_4 does not follow any of the standard trends for a size-mismatch-based phenomenon. We must conclude, therefore, that this peak in the hardness is due to changes in the structure and bonding of WB_4 when doped with Mo.

In our previous study,[23] we attributed the sharp peaks observed in the Vickers hardness data for Ta- and Mn-doped WB_4 at low concentrations (∼2 at. % Ta or 4 at. % Mn) to an electronic structure effect. Located in different columns of the Periodic Table, Ta (group 5) and Mn (group 7) each have a different number of valence electrons compared to W (group 6), imposing a change in the Fermi level of WB_4 when they substitute for W atoms. Either raising or lowering the valence electron counts, compared to W, should change the overall valence electron concentration (VEC)[21] as one varies the concentration of Ta or Mn in WB_4.[27] This, in turn, can change the mechanical properties, likely by influencing the strength of various metal−boron or metal−metal bonds in the system.[22] Because the cohesive energy of a metallic solid is very sensitive to the details of the Fermi energy, the appearance of the sharp peaks in concentration-dependent hardness of WB_4−Ta and WB_4−Mn at low concentrations seems reasonable.[23] These low concentrations may approach the optimal dopant levels that cause complete filling of σ-bonding states between the d orbitals of the metals and the p orbitals of boron. Such doping would thus maximize the bond covalency.[21,22] Note that we could not verify the presence or absence of a low-concentration peak in the WB_4−Cr system in our previous study because of the overlap of such a peak with the observed hardness resulting from the limited solubility of Cr in WB_4 (<10 at. %). Because of the isoelectronic nature of W and Cr, it was assumed that no such peak existed, but the question can be resolved using our current electronically comparable system, WB_4−Mo, since W, Cr, and Mo are all isoelectronic (group 6).

Here we find that upon addition of small amounts of Mo to WB_4, the sharp peak is still observed in the Mo-concentration-dependent hardness (Figure 2) at a low concentration of ∼3 at. % Mo. To understand this result, we must first consider the unique crystal structure of WB_4. We have very recently shown, using neutron diffraction experiments, that the structure of WB_4 consists of alternating hexagonal layers of boron and tungsten atoms, with some tungsten atoms (1/3) missing and their positions occupied by boron trimers.[18] Since both Mo and W have the same number of valence electrons (group 6), one would not expect to see this peak unless the atoms of Mo substitute for the boron trimers rather than for W atoms. The difference between the number of valence electrons for Mo and for boron trimers could change the total VEC and again result in stronger metal−boron bonds, leading to enhanced hardness. We note that the VEC is theoretically predicted to be optimized at around a 3% change, in good agreement with our results.[21] In support of this idea, we note that, in contrast to the system examined here, $Os_{1-x}Ru_xB_2$ solid solutions,[22] which also contain two elements from the same group of the Periodic Table (ruthenium (Ru) and osmium (Os), both group 8), show no enhancement in hardening due to electronic structure changes. The structure of the $Os_{1-x}Ru_xB_2$ system is much simpler than WB_4, however, and has no sites that can be occupied by either metal or by boron. As a result, in that system, it therefore appears that the Fermi level remains constant, regardless of the dopant concentration. Hence, it appears that the unique structure of WB_4, with sites that can be occupied either by metal atoms or by boron trimers, allows for remarkable enhancements in hardness at very low heteroatom doping levels.

After substitution for some of the boron trimers, as the concentration of Mo in WB_4 exceeds ∼3 at. %, the molybdenum atoms likely begin substituting for tungsten atoms in the lattice, causing the linear hardness trends seen in Figure 2. For this region (5−50 at. % Mo), it seems that the solid solutions mostly follow Vegard's law with a very low slope, as the atoms of W and Mo have similar radii and equal valence electron counts. Therefore, the size mismatch and the change in the energy profile of nearest neighbors are expected to be small, maintaining the symmetric motion of natural dislocations and making Vegard's law dominant in the hardness behavior of this system at medium-to-high dopant concentrations.

On the basis of these results, we suggest that the relatively broad peak that we observed in the Cr-concentration-dependent Vickers hardness curves for the WB_4−Cr system below ∼10 at. % Cr in our past study[23] may well have been due

DOI: 10.1021/acs.chemmater.5b04410
Chem. Mater. 2016, 28, 632−637

to the overlap of two solid-solution hardening mechanisms: an electronic structure change due to the substitution of Cr for boron trimers, similar to the WB_4–Mo system, and hardening due to the atomic size mismatch between W (1.41 Å) and Cr (1.30 Å). Moreover, in previously studied systems with a difference in electron count (WB_4–Mn and WB_4–Ta), it may be that substitution of Mn and Ta for boron trimers also played a significant role.

It is interesting to speculate about the trends in hardness for Mo concentrations above 50 at. % Mo, as the structure moves gradually from WB_4 toward MoB_4 (known as $Mo_{0.8}B_3$, hexagonal $P6_3/mmc$).[25] On the basis of the data of Figure 2, we interpret that the hardness should likely fall on a flat line sloping slightly downward, that is, following Vegard's law. This is because the crystal structures and lattice constants of both end members (WB_4 and MoB_4) are very similar.[2,25,28] Mo atoms have less electron density than W atoms, however, and this should lead to reduced electronic repulsion in MoB_4 compared to that in WB_4, and thus lower hardness for MoB_4.[29] Similar behavior has been observed for other hard solid solutions.[22,30,31] By linearly extrapolating the hardness data shown here for the WB_4–Mo system (Figure 2) beyond 50 at. % Mo, we estimate hardness values of ~23.9 and 35.9 GPa for MoB_4 under applied loads of 4.90 and 0.49 N, respectively. Note that our attempts to synthesize phase-pure MoB_4 by arc melting, even in the presence of excess boron, were not successful due to the formation of the thermodynamically favorable phase molybdenum diboride (MoB_2).[32] Also, to our knowledge, no reliable experimental or theoretical data are available in the literature for the hardness of MoB_4.

In an effort to further assess the suitability of these materials for applications such as cutting, the thermal stability of the hardest solid solution of WB_4 with Mo, $W_{0.97}Mo_{0.03}B_4$, is compared to that of WC in Figure 3. Figure 3 shows that both

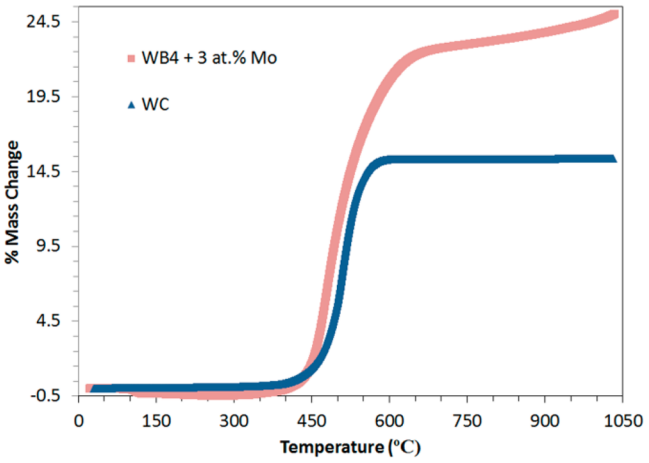

Figure 3. Thermal stability of the hardest solid solution of WB_4 with Mo, $W_{0.97}Mo_{0.03}B_4$, compared to the traditional cutting tool material, WC. It is observed that both materials are thermally stable in air up to ~400 °C.

materials are thermally stable in air up to ~400 °C, which is similar to that of pure WB_4.[16] The products of the thermal reactions include WO_3 and $B(OH)_3$ for $W_{0.97}Mo_{0.03}B_4$ and WO_3 for WC, as identified by powder X-ray diffraction. The higher weight gain for $W_{0.97}Mo_{0.03}B_4$ may be due to the formation of $B(OH)_3$ (boric acid) in $W_{0.97}Mo_{0.03}B_4$ while WC likely forms the gaseous product CO_2, which is lost during the thermal oxidation reaction. Thermal stability is important in cutting tool applications, where the local temperature can exceed several hundred degrees Celsius.

4. CONCLUSIONS

By successfully synthesizing WB_4 solid solutions with Mo and taking a systematic approach to the study of their Vickers hardness, we have demonstrated that the hardness of superhard transition-metal borides can be enhanced by creating solid solutions with other transition metals, even metals that are isoelectronic with the parent. These solid solutions compare favorably to previously synthesized superhard metal borides (Table 2). We found that the Vickers hardness, under applied loads of 4.90 and 0.49 N, respectively, increases from 28.1 and 43.3 GPa for pure WB_4 to 33.4 and 50.3 GPa for the solid solution containing 3 at. % Mo. This solid solution ($W_{0.97}Mo_{0.03}B_4$) is thermally stable up to ~400 °C in air, and therefore has potential as a substitute for WC in tool applications. The results of this study suggest that not only can one metal substitute for another in the WB_4 crystal structure but also metals can substitute for boron trimers, thus changing the electronic structure of the lattice and resulting in a different type of solid-solution hardening. This new possibility of substituting metals for boron may change our criteria for designing new superhard borides based on our understanding of their structures and possible hardening mechanisms.

Table 2. Hardness (H_v), Bulk Modulus (K_{0T}), Shear Modulus (G), and Young's Modulus (E) of Selected Superhard Metal Borides

compound	H_v (GPa)	K_{0T} (GPa)	G (GPa)	E (GPa)
ReB_2	30–48[3]	344[5]	267[3]	614[3]
WB_4	28–43[16]	326[23]	245[33]	553[16]
$W_{0.93}Ta_{0.02}Cr_{0.05}B_4$	32–57[23]	335[23]		
$W_{0.97}Mo_{0.03}B_4$ (this work)	33–50			

AUTHOR INFORMATION

Corresponding Authors

*E-mail: kaner@chem.ucla.edu.

*E-mail: rmohammadi@vcu.edu.

Notes

The authors declare no competing financial interest.

ACKNOWLEDGMENTS

The authors thank Prof. Benjamin M. Wu at the UCLA Department of Materials Science and Engineering for use of his microindentation system. Financial support for this research from the National Science Foundation under grants 1106364 and 1506860 (SHT and RBK) and the Natural Science and Engineering Council of Canada (RM) is gratefully acknowledged. R.M. is also thankful for the VCU Startup Grant (137422).

REFERENCES

(1) Kaner, R. B.; Gilman, J. J.; Tolbert, S. H. Materials Science-Designing Superhard Materials. *Science* **2005**, *308*, 1268–1269.

(2) Levine, J. B.; Tolbert, S. H.; Kaner, R. B. Advancements in the Search for Superhard Ultra-Incompressible Metal Borides. *Adv. Funct. Mater.* **2009**, *19*, 3519–3533.

(3) Mohammadi, R.; Kaner, R. B. Superhard Materials. In *Encyclopedia of Inorganic and Bioinorganic Chemistry*; Scott, R. A.,

DOI: 10.1021/acs.chemmater.5b04410
Chem. Mater. 2016, 28, 632–637

Ed.; John Wiley: Chichester, 2012; DOI: 10.1002/9781119951438.eibc2076.
(4) Chung, H. Y.; Weinberger, M. B.; Yang, J. M.; Tolbert, S. H.; Kaner, R. B. Correlation between Hardness and Elastic Moduli of the Ultraincompressible Transition Metal Diborides RuB_2, OsB_2, and ReB_2. *Appl. Phys. Lett.* **2008**, *92*, 261904.
(5) Chung, H. Y.; Weinberger, M. B.; Levine, J. B.; Kavner, A.; Yang, J. M.; Tolbert, S. H.; Kaner, R. B. Synthesis of Ultra-Incompressible Superhard Rhenium Diboride at Ambient Pressure. *Science* **2007**, *316*, 436−439.
(6) Levine, J. B.; Nguyen, S. L.; Rasool, H. I.; Wright, J. A.; Brown, S. E.; Kaner, R. B. Preparation and Properties of Metallic, Superhard Rhenium Diboride Crystals. *J. Am. Chem. Soc.* **2008**, *130*, 16953−16958.
(7) Levine, J. B.; Betts, J. B.; Garrett, J. D.; Guo, S. Q.; Eng, J. T.; Migliori, A.; Kaner, R. B. Full Elastic Tensor of a Crystal of the Superhard Compound ReB_2. *Acta Mater.* **2010**, *58*, 1530−1535.
(8) Tkachev, S. N.; Levine, J. B.; Kisliuk, A.; Sokolov, A. P.; Guo, S. Q.; Eng, J. T.; Kaner, R. B. Shear Modulus of Polycrystalline Rhenium Diboride Determined from Surface Brillouin Spectroscopy. *Adv. Mater.* **2009**, *21*, 4284−4286.
(9) Suzuki, Y.; Levine, J. B.; Migliori, A.; Garrett, J. D.; Kaner, R. B.; Fanelli, V. R.; Betts, J. B. Rhenium Diboride's Monocrystal Elastic Constants. *J. Acoust. Soc. Am.* **2010**, *127*, 2797−2801.
(10) Romans, P. A.; Krug, M. P. Composition and Crystallographic Data for the Highest Boride of Tungsten. *Acta Crystallogr.* **1966**, *20*, 313−315.
(11) Itoh, H.; Matsudaira, T.; Naka, S.; Hamamoto, H.; Obayashi, M. Formation Process of Tungsten Borides by Solid State Reaction between Tungsten and Amorphous Boron. *J. Mater. Sci.* **1987**, *22*, 2811−2815.
(12) Brazhkin, V. V.; Lyapin, A. G.; Hemley, R. J. Harder than Diamond: Dreams and Reality. *Philos. Mag. A* **2002**, *82*, 231−253.
(13) Gu, Q.; Krauss, G.; Steurer, W. Transition Metal Borides: Superhard versus Ultra-Incompressible. *Adv. Mater.* **2008**, *20*, 3620−3626.
(14) Liu, C.; Peng, F.; Tan, N.; Liu, J.; Li, F.; Qin, J.; Wang, J.; Wang, Q.; He, D. Low-Compressibility of Tungsten Tetraboride: a High Pressure X-ray Diffraction Study. *High Pressure Res.* **2011**, *31*, 275−282.
(15) Rau, J. V.; Latini, A.; Teghil, R.; De Bonis, A.; Fosca, M.; Caminiti, R.; Rossi Albertini, V. Superhard Tungsten Tetraboride Films Prepared by Pulsed Laser Deposition Method. *ACS Appl. Mater. Interfaces* **2011**, *3*, 3738−3743.
(16) Mohammadi, R.; Lech, A. T.; Xie, M.; Weaver, B. E.; Yeung, M. T.; Tolbert, S. H.; Kaner, R. B. Tungsten Tetraboride, an Inexpensive Superhard Material. *Proc. Natl. Acad. Sci. U. S. A.* **2011**, *108*, 10958−10962.
(17) Xie, M.; Mohammadi, R.; Mao, Z.; Armentrout, M. M.; Kavner, A.; Kaner, R. B.; Tolbert, S. H. Exploring the High-Pressure Behavior of Superhard Tungsten Tetraboride. *Phys. Rev. B: Condens. Matter Mater. Phys.* **2012**, *85*, 064118.
(18) Lech, A. T.; Turner, C. L.; Mohammadi, R.; Tolbert, S. H.; Kaner, R. B. Structure of Superhard Tungsten Tetraboride: A Missing Link between MB_2 and MB_{12} Higher Borides. *Proc. Natl. Acad. Sci. U. S. A.* **2015**, *112*, 3223−3228.
(19) Dieter, G. E. *Mechanical Metallurgy*; McGraw Hill: New York, 1986.
(20) Sha, J. B.; Yamabe-Mitarai, Y. Saturated Solid-Solution Hardening Behavior of Ir-Hf-Nb Refractory Superalloys for Ultra-High Temperature Applications. *Scr. Mater.* **2006**, *54*, 115−119.
(21) Jhi, S. H.; Ihm, J.; Louie, S. G.; Cohen, M. L. Electronic Mechanism of Hardness Enhancement in Transition-Metal Carbonitrides. *Nature* **1999**, *399*, 132−134.
(22) Weinberger, M. B.; Levine, J. B.; Chung, H. Y.; Cumberland, R. W.; Rasool, H.; Yang, J. M.; Kaner, R. B.; Tolbert, S. H. Incompressibility and Hardness of Solid Solution Transition Metal Diborides: $Os_{1-x}Ru_xB_2$. *Chem. Mater.* **2009**, *21*, 1915−1921.
(23) Mohammadi, R.; Xie, M.; Lech, A. T.; Turner, C. L.; Kavner, A.; Tolbert, S. H.; Kaner, R. B. Toward Inexpensive Superhard Materials: Tungsten Tetraboride-Based Solid Solutions. *J. Am. Chem. Soc.* **2012**, *134*, 20660−20668.
(24) Egami, T.; Waseda, Y. Atomic Size Effect on the Formability of Metallic Glasses. *J. Non-Cryst. Solids* **1984**, *64*, 113−134.
(25) Lundstrom, T.; Rosenberg, I. The Crystal Structure of the Molybdenum Boride $Mo_{1-x}B_3$. *J. Solid State Chem.* **1973**, *6*, 299−305.
(26) Zhou, Y. C.; Chen, J. X.; Wang, J. Y. Strengthening of Ti_3AlC_2 by Incorporation of Si to Form $Ti_3Al_{1-x}Si_xC_2$ Solid Solutions. *Acta Mater.* **2006**, *54*, 1317−1322.
(27) Gou, H.; Li, Z.; Wang, L. M.; Lian, J.; Wang, Y. Peculiar Structure and Tensile Strength of WB_4: Nonstoichiometric Origin. *AIP Adv.* **2012**, *2*, 012171.
(28) Wang, M.; Li, Y. W.; Cui, T.; Ma, Y. M.; Zou, G. T. Origin of Hardness in WB_4 and Its Implications for ReB_4, TaB_4, MoB_4, TcB_4, and OsB_4. *Appl. Phys. Lett.* **2008**, *93*, 101905.
(29) Hoffman, D. C.; Lee, D. M. Chemistry of the Heaviest Elements − One Atom at a Time. *J. Chem. Educ.* **1999**, *76*, 331−347.
(30) Pershina, V.; Bastug, T.; Fricke, B. Relativistic Effects on the Electronic Structure and Volatility of Group-8 Tetraoxides MO4, Where M = Ru, Os, and Element 108, Hs. *J. Chem. Phys.* **2005**, *122*, 124301.
(31) Onoe, J. Relativistic Effects on Covalent Bonding: Role of Individual Valence Atomic Orbitals. *J. Phys. Soc. Jpn.* **1997**, *66*, 2328−2336.
(32) *ASM Handbook, Vol. 3: Alloy Phase Diagrams, 10th Ed.*; ASM International: Materials Park, OH, 1992.
(33) Zhang, R. F.; Legut, Z. D.; Lin, J.; Zhao, Y. S.; Mao, H. K.; Veprek, S. Stability and Strength of Transition-Metal Tetraborides and Triborides. *Phys. Rev. Lett.* **2012**, *108*, 255502.

DOI: 10.1021/acs.chemmater.5b04410
Chem. Mater. 2016, 28, 632−637